ResearchGate

See discussions, stats, and author profiles for this publication at: https://www.researchgate.net/publication/221850077

# Microstructure Evolution and Device Performance in Solution-Processed Polymeric Field-Effect Transistors: The Key Role of the First Monolayer

**ARTICLE** *in* JOURNAL OF THE AMERICAN CHEMICAL SOCIETY · MARCH 2012

Impact Factor: 12.11 · DOI: 10.1021/ja211630w · Source: PubMed

CITATIONS
51

READS
75

**4 AUTHORS**, INCLUDING:

Suhao Wang
Linköping University
**17** PUBLICATIONS **347** CITATIONS
SEE PROFILE

Adam Kiersnowski
Wroclaw University of Technology
**33** PUBLICATIONS **323** CITATIONS
SEE PROFILE

Wojciech Pisula
Max Planck Institute for Polymer Research
**213** PUBLICATIONS **8,884** CITATIONS
SEE PROFILE

Available from: Adam Kiersnowski
Retrieved on: 17 January 2016

JACS
JOURNAL OF THE AMERICAN CHEMICAL SOCIETY

Communication

pubs.acs.org/JACS

# Microstructure Evolution and Device Performance in Solution-Processed Polymeric Field-Effect Transistors: The Key Role of the First Monolayer

Suhao Wang,[†] Adam Kiersnowski,[†,‡] Wojciech Pisula,*[,†] and Klaus Müllen*[,†]

[†]Max Planck Institute for Polymer Research, Ackermannweg 10, 55128 Mainz, Germany

[‡]Polymer Engineering and Technology Division, Wroclaw University of Technology, Wybrzeze Wyspianskiego 27, 50-370 Wroclaw, Poland

Supporting Information

**ABSTRACT:** Probing the role of the first monolayer in the evolution of the film polymer microstructure is essential for the fundamental understanding of the charge carrier transport in polymeric field-effect transistors (FETs). The monolayer and its subsequent microstructure of a conjugated polymer [poly(2,5-bis(3-alkylthiophen-2-yl)thieno[3,2-*b*]thiophene), **PBTTT**] film were fabricated via solution deposition by tuning the dip-coating speed and were then studied as accumulation and transporting layers in FETs. Investigation of the microstructure of the layers prepared at different coating velocities revealed that the monolayer serves as an important base for further development of the film. Significant improvement of the charge carrier transport occurs only at a critical multilayer network density that establishes the required percolation pathways for the charge carriers. Finally, at a low dip-coating speed, the polymer chains are uniaxially oriented, yielding pronounced structural anisotropy and high charge carrier mobilities of 1.3 $cm^2\ V^{-1}\ s^{-1}$ in the alignment direction.

During the past decade, organic field-effect transistors (OFETs) have attracted considerable attention because of their potential applications in large-area, low-cost, flexible electronic devices, such as flexible electronic paper, radio-frequency identification (RFID) tags, postage stamps, and backplane circuitry for active-matrix displays.[1] Particularly, ultrathin-film OFETs with few semiconducting monolayers are of vital importance, because charge carriers are directly transported to conduction channels without diffusion through a dense film. For small conjugated molecules[2a−i] and very recently for a conjugated polymer,[2j] it has been proven that the main charge carrier transport in transistors occurs in a few molecular layers near the dielectric surface. This is also in line with the theory that predicts a high density of charges and thus high charge carrier mobility in the first few nanometers of the active film.[2k] Therefore, particular emphasis was put on the molecular order within this thin accumulation layer processed, for example, by vacuum deposition,[2b,f] Langmuir−Blodgett deposition,[2c] and electrostatic force-based self-assembly.[2d] Little is known, however, about the influence of solution processing (considered to be the future process in roll-to-roll fabrication of electronic devices) on the molecular organization in ultrathin films after solvent evaporation.

There have been only few studies on conjugated polymers in ultrathin-film FETs, consisting of multilayers of poly(3-hexylthiophene)[3a,b,d] and polydiacetylene.[3c] Both cases showed a performance far inferior to the corresponding thick-film OFETs, proving that potential applications are a long way off. The solution processing of conjugated polymers into one single monolayer and its subsequent layers directly on the surface in a FET channel is a great challenge and therefore has been rarely reported to date. Especially, technical questions concerning precise bottom-up solution growth of a conjugated polymer from monolayer to multilayer still need to be answered. This would allow a fundamental study of the role of the first monolayer on the evolution of the bulk polymer microstructure and the charge carrier transport in the transistor.

This communication reports the early stages of polymer film formation that is precisely controlled via a facile dip-coating process by tuning the pulling speed of the substrate from the solution reservoir. As a model compound, the well-known high-performance p-type polymer poly(2,5-bis(3-alkylthiophen-2-yl)thieno[3,2-*b*]thiophene) (**PBTTT**, Scheme 1) was used.[1d] A monolayer and the subsequent microstructure of a conjugated polymer on a rigid OFET surface were successfully obtained from solution. We prove that the first monolayer has essential importance for the bulk microstructure evolution, whereby a critical multilayer network is necessary for creating the required percolation pathways for the charge carriers in thin-film polymer OFETs.

**Scheme 1. Molecular Structure of PBTTT**

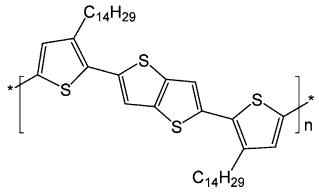


During the dip-coating process, the pulling speed was gradually changed and had a great impact on the growth of

**Received:** December 13, 2011
**Published:** February 21, 2012

 © 2012 American Chemical Society  dx.doi.org/10.1021/ja211630w | *J. Am. Chem. Soc.* 2012, 134, 4015−4018

**PBTTT**, mainly on the network density in the corresponding molecular layers as well as on their different morphology development. Remarkably, the monolayer and a subsequent network were formed over large areas by dip-coating, as proven by atomic force microscopy (AFM) images (Figure 1).

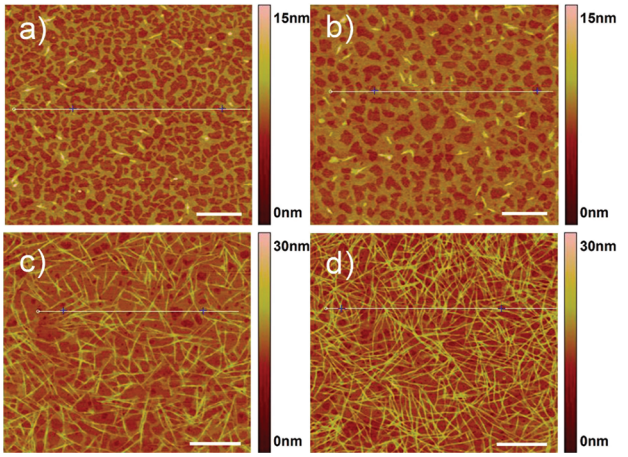


**Figure 1.** Tapping-mode AFM images of **PBTTT** on a $SiO_2$ surface obtained by dip-coating under different pulling speeds: (a) 1 mm/s; (b) 200 $\mu$m/s; (c) 40 $\mu$m/s; (d) 10 $\mu$m/s. The white lines in the AFM images correspond to the height profiles in Figure S1. Scale bars: (a, b) 500 nm; (c, d) 1 $\mu$m.

As shown in Figure 1a and Figure S1a in the Supporting Information (SI), a discontinuous monolayer network of **PBTTT** with a thickness of 1.8 nm was formed on $SiO_2$ surface when the substrate was pulled at the highest speed of 1 mm/s. This height is in agreement with the chain-to-chain distance determined by X-ray scattering for a bulk film (see below). On top of this 2D monolayer, 1D fiber nuclei (thickness of 4–6 nm) started to grow only on top of the **PBTTT** monolayer and not on the $SiO_2$ surface (Figure 1a). This is noteworthy since the subsequent microstructure began to develop while the first monolayer was not fully established (~30% coverage). Moreover, a striking difference between the first layer and the subsequent microstructure was obvious and is attributed to the different surface tensions of **PBTTT** molecules and $SiO_2$. The differences in the contact angle were <10° for $SiO_2$ and 102 ± 1° for the **PBTTT** layer. More precisely, in comparison to bare $SiO_2$ surface, the long alkyl chains of **PBTTT** lead to stronger hydrophobic interactions between the deposited polymer and the first layer.[4] As a result, **PBTTT** self-assembles into isolated anisotropic 1D fibers on top of the first monolayer. The phenomenon of different morphologies for the first monolayer and the subsequent microstructures is analogous to the previous findings on small molecules.[5,2f] For instance, in the case of pentacene, the first monolayer shows a higher nucleation density than the subsequent monolayers, since the diffusion coefficient of pentacene molecules on $SiO_2$ is lower than that on pentacene.[5]

The well-controlled growth of the polymer film allowed a systematic investigation of the charge carrier transport in the charge accumulation and transporting layer of an OFET. Details of the device fabrication are described in the SI. The OFET devices were studied only in a top-contact configuration to exclude differences in surface energy between bottom Au electrodes and the $SiO_2$ surface and to avoid any discontinuities in the film. For instance, in the case of untreated $SiO_2$, nucleation of pentacene takes place preferentially at the electrodes, which causes discontinuities and clustering in the pentacene film.[2f] Almost no field-effect characteristics (<$10^{-6}$ $cm^2$ $V^{-1}$ $s^{-1}$) were observed for the monolayer shown in Figure 1a. It must be emphasized that a prerequisite for efficient charge carrier transport is a continuous long-range percolation path between the source and drain electrodes with intimately connected molecules. However, this is not the case for the layer in Figure 1a.

Decreasing the pulling speed to 200 $\mu$m/s led to coverage of a larger area by the first monolayer and therefore a more continuous film (Figure 1b and Figure S1b). In addition, the subsequent fiber nuclei (thickness does not change) became longer but were still not interconnected. The extended first monolayer and grown subsequent fiber nuclei are attributed to

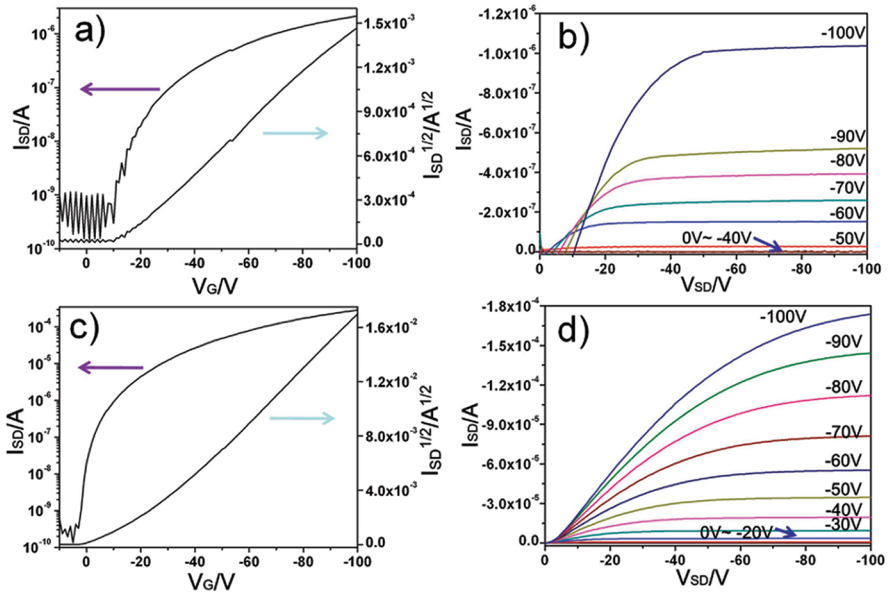


**Figure 2.** (a, c) Transfer and (b, d) output curves corresponding to the **PBTTT** films processed by dip-coating at (a, b) 40 and (c, d) 10 $\mu$m/s.


dx.doi.org/10.1021/ja211630w | *J. Am. Chem. Soc.* 2012, 134, 4015–4018

the lower substrate speed, which ensures the availability of more molecules for building up the microstructures on the $SiO_2$ surface. It is also known from the literature that only an ineffective connection between the electrodes and a single layer of molecules can be achieved, limiting the charge carrier injection.[6] These are the reasons for a low charge carrier mobility of $1.6 \times 10^{-4}$ $cm^2$ $V^{-1}$ $s^{-1}$ and on/off ratio of $\sim 10^2$ for the corresponding transistor (Figure S2). A further proof of ineffective charge carrier injection is the relatively high threshold voltage of −20 V. These results are in agreement with previous findings showing that a monolayer of a small molecular semiconductor is not sufficient for high performance.[6] Despite the low performance, we define this mobility as an onset value for a minimal film thickness/microstructure of **PBTTT** for a working transistor.

With a further decrease in the pulling speed to 40 μm/s, the **PBTTT** monolayer almost completely covered the $SiO_2$ surface (Figure 1c). In comparison to Figure 1b, the nucleation centers of the subsequent microstructure further developed into long fibers that formed a dense network with interconnections. As a result, the charge carrier mobility was 1 order of magnitude higher, $2.0 \times 10^{-3}$ $cm^2$ $V^{-1}$ $s^{-1}$, with an on/off ratio of $\sim 10^4$ in comparison to the previous film. (Figure 2a,b) Additionally, the threshold voltage was reduced from −20 V to −12 V. The effect of contact resistance and problems with charge injection were clearly indicated by both the transfer and output curves. (Figure 2a,b)

When the speed of the substrate was further reduced to 10 μm/s, a closed first layer and a continuous subsequent fibrous multilayer were obtained (Figure 1d). As shown in Figure 2c,d, a mobility of 0.36 $cm^2$ $V^{-1}$ $s^{-1}$ with an on/off ratio of $1 \times 10^6$ were determined. Moreover, the threshold voltage was again lowered, from −12 V to −5 V. The significantly improved mobility and threshold voltage of this multilayer are attributed to the formation of a dense fibrous network layer. Such a network structure is ideal for OFET applications because the interconnected fiber structure enhances the charge carrier transport within the FET channel.

Finally, at the lowest speed of 2 μm/s, long-range-aligned, continuous polymer fibrous layers were obtained for films with a total thickness of ∼15 nm over a macroscopic scale (Figure 3a and Figure S3). This pronounced orientation was induced by the low pulling speed and by the gradient established in the meniscus at the solvent−substrate interface. We previously proved that under optimized dip-coating conditions (e.g., low pulling speed), conjugated donor−acceptor polymer chains are directed in the processing direction, in which the maximum charge carrier mobility was recorded.[7] Previously, **PBTTT** was oriented via a flow-coating method.[8] In the case of dip-coating at 2 μm/s, the long-range-aligned **PBTTT** films yielded a high average mobility of $0.7 \pm 0.2$ $cm^2$ $V^{-1}$ $s^{-1}$ with a highest mobility of 1.3 $cm^2$ $V^{-1}$ $s^{-1}$ and a current on/off ratio of $5 \times 10^6$ measured parallel to the coating direction. It must be emphasized that this value is the highest published to date for **PBTTT**-based FETs. Remarkably enough, the dip-coated films were simply deposited on untreated $SiO_2$ dielectric, which is known as serious charge carrier trap.[9] Furthermore, the films were annealed far below the liquid-crystalline phase transition, above which typically the molecular packing improves significantly and for **PBTTT** leads to better device performance. In this case, however, the film dewetted at an annealing temperature of 180 °C because of the low thickness, forming a discontinuous network (Figure S5) and revealing much lower charge carrier mobility of 0.02 $cm^2$ $V^{-1}$ $s^{-1}$. Such a film topography of **PBTTT** after heating to the liquid-crystalline phase is in agreement with the literature.[10] Another remarkable effect is the pronounced anisotropy of the electronic properties. The FET measurement perpendicular to the alignment direction gave charge carrier mobilities of only $6.2 \times 10^{-2}$ $cm^2$ $V^{-1}$ $s^{-1}$. This is a significantly larger anisotropy ratio of ∼20 in comparison with the value of ∼2 in our previous work on a donor−acceptor polymer.[7] To prove the structural isotropy for the layers processed at 10 μm/s or faster relative to the anisotropy obtained by dip-coating at 2 μm/s, the films were studied by grazing-incidence wide-angle X-ray scattering (GIWAXS). All of the patterns revealed reflections on the $q_z$ line having identical positions characteristic of a chain-to-chain distance of 2.2 nm between edge-on arranged **PBTTT** polymer chains (Figure S4). However, differences were obvious for the reflections attributed to the π-stacking of 0.38 nm, which were located on the $q_y$ line. Because of the uniaxial orientation of the conjugated polymers along the drawing direction of the substrate at the processing speed of 2 μm/s, the scattering intensity was significantly higher for the measurement parallel to the dip-coating direction, while it disappeared when the sample was investigated perpendicular to this direction (Figure 3b). In contrast to this, the intensities of the π-stacking reflections in the two directions were the same for the film processed at 10 μm/s (Figure 3c), confirming the structural isotropy. This isotropy is in good agreement with the microstructure in the AFM image in Figure 1d.

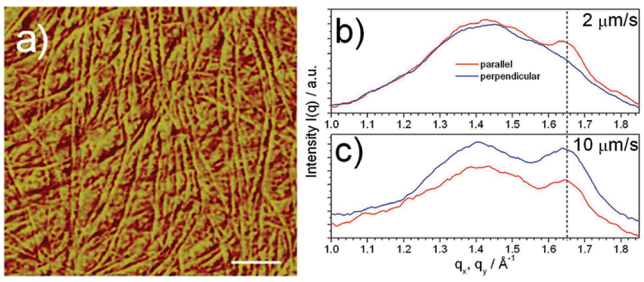


**Figure 3.** (a) AFM image of the uniaxially oriented film dip-coated at 2 μm/s (the scale bar corresponds to 1 μm). (b, c) $q_x/q_y$ integrations for the scattered intensities recorded perpendicular (blue) and parallel (red) to the dip direction. Films were obtained at (b) 2 μm/s and (c) 10 μm/s. The dashed lines indicate the position of π-stacking reflections.

The GIWAXS analysis allowed us to develop the following model for the organization in the various layers of the thin film, which is presented schematically in Figure 4. The monolayer at the dielectric surface consists of edge-on arranged polymer chains, as suggested by the AFM images. On top of this first layer, fibers are formed in which the edge-on polymer backbones are oriented along the fiber axis. This corresponds also to the growth fiber direction and the faster charge carrier migration. In these 4−6 nm thick fibers, the polymer out-of-plane chain-to-chain spacing is 2.2 nm, which is in a range identical to the monolayer thickness. This means that in the fiber two or three polymer chains are arranged on top of each other as illustrated in Figure 4.

In conclusion, a monolayer and the subsequent microstructure of a conjugated polymer on a rigid surface can be precisely controlled by dip-coating. These results point toward an essential role of the first polymer monolayer on the


dx.doi.org/10.1021/ja211630w | J. Am. Chem. Soc. 2012, 134, 4015−4018

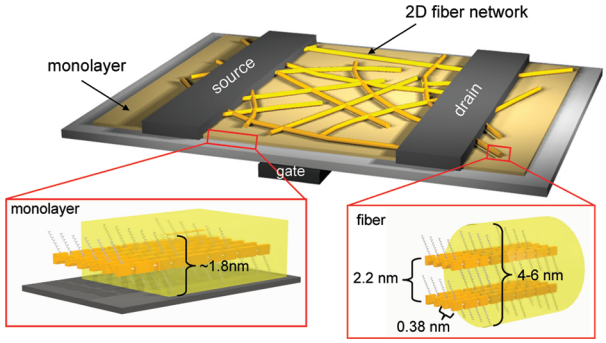


**Figure 4.** Schematic illustration of the molecular organization in the thin film deposited at 10 $\mu$m/s in an OFET.

microstructure evolution in the bulk film during solution processing and on the charge carrier transport in the transistor. For a sufficient charge carrier transport, a critical multilayer network is necessary to create the required percolation pathways. Our approach opens a new pathway for the bottom-up fabrication of conjugated polymer ultrathin films and provides new insights into the fundamental understanding of solution-processable OFETs based on polymer thin films. Currently, we are clarifying the question of the degree to which these findings can be generalized to other conjugated polymers. Since the self-assembly of polymers strongly depends on the design of the backbone and the attached substituents, differences in the development of the film structure could be expected for other systems. The same question arises concerning the solution deposition technique with different processing parameters. Our preliminary AFM images (Figure S6) for spin-coated films indicate that a mechanism identical to that for dip-coating takes place during the microstructure evolution. Long, thick fibers were formed on top of a layer of **PBTTT**. Unfortunately, spin-coating does not allow defined control of the process conditions as in the case of dip-coating. Our future work will focus on the verification of these conclusions for other conjugated, solution-processed systems and different processing techniques.

## ■ ASSOCIATED CONTENT

### Ⓢ Supporting Information

Experimental procedures, dip-coating process, AFM image for the annealed film, AFM height profiles, and GIWAXS patterns. This material is available free of charge via the Internet at http://pubs.acs.org.

## ■ AUTHOR INFORMATION

### Corresponding Author

pisula@mpip-mainz.mpg.de; muellen@mpip-mainz.mpg.de

### Notes

The authors declare no competing financial interest.

## ■ ACKNOWLEDGMENTS

Support was provided by the German Science Foundation (Korean–German IR TG), the European Community's Seventh Framework Programme ONE-P (Grant Agreement 212311), DFG Priority Program SPP 1355, DFG MU 334/32-1, DFG Priority Program SPP 1459, and ESF Project GOSPEL (09-EuroGRAPHENE-FP-001). A.K. acknowledges support from the Marie Curie Intra European Fellowship (PIEF-GA-2009-253521) granted within Seventh EU Framework Program.

## ■ REFERENCES

(1) (a) Sirringhaus, H.; Tessler, N.; Friend, R. H. *Science* **1998**, *280*, 1741. (b) Huitena, H. E. A.; Gelinck, G. H.; van der Putter, J. B. P. H.; Kuijk, K. E.; Hart, C. M.; Cantatore, E.; Herwig, P. T.; van Breemen, A. J. J. M.; de Leeuw, D. M. *Nature* **2001**, *414*, 599. (c) Facchetti, A.; Yoon, M.; Marks, T. J. *Adv. Mater.* **2005**, *17*, 1705. (d) McCulloch, I.; Heeney, M.; Bailey, C.; Genevicius, K.; MacDonald, I.; Shkunov, M.; Sparrowe, D.; Tierney, S.; Wagner, R.; Zhang, W.; Chabinyc, M. L.; Kline, J. R.; McGehee, M. D.; Toney, M. F. *Nat. Mater.* **2006**, *5*, 328–333. (e) Berggren, M.; Nilsson, D.; Robinson, N. D. *Nat. Mater.* **2007**, *6*, 3. (f) Liu, S.; Wang, W. M.; Briseno, A. L.; Mannsfeld, S. C. B.; Bao, Z. *Adv. Mater.* **2009**, *21*, 1217. (g) Di, C.; Liu, Y.; Yu, G.; Zhu, D. *Acc. Chem. Res.* **2009**, *42*, 1573. (h) Tsao, H. N.; Müllen, K. *Chem. Soc. Rev.* **2010**, *39*, 2372. (i) Facchetti, A. *Chem. Mater.* **2011**, *23*, 733.

(2) (a) Dodabalapur, A.; Torsi, L.; Katz, H. *Science* **1995**, *268*, 270. (b) Sirringhaus, H.; Brown, P. J.; Friend, R. H.; Nielsen, M. M.; Bechgaard, K.; Langeveld-Voss, B. M. W.; Spiering, A. J. H.; Janssen, R. A. J.; Meijer, E. W.; Herwig, P.; de Leeuw, D. M. *Nature* **1999**, *401*, 685. (c) Xiao, K.; Liu, Y. Q.; Huang, X. B.; Xu, Y.; Yu, G.; Zhu, D. B. *J. Phys. Chem. B* **2003**, *107*, 9226. (d) Locklin, J.; Shino, K.; Onishi, K.; Kaneko, F.; Bao, Z. N.; Advincula, R. C. *Chem. Mater.* **2003**, *15*, 1404. (e) Dinelli, F.; Murgia, M.; Levy, P.; Cavallini, M.; Biscarini, F.; de Leeuw, D. M. *Phys. Rev. Lett.* **2004**, *92*, No. 116802. (f) Ruiz, A.; Papadimitratos, A.; Mayer, A. C.; Malliaras, G. G. *Adv. Mater.* **2005**, *17*, 1795. (g) Huang, J.; Sun, J.; Katz, H. E. *Adv. Mater.* **2008**, *20*, 2567. (h) Mathijssen, S. G. J.; Smits, E. C. P.; van Hal, P. A.; Wondergem, H. J.; Ponomarenko, S. A.; Moser, A.; Resel, R.; Bobbert, P. A.; Kemerink, M.; Janssen, R. A. J.; de Leeuw, D. M. *Nat. Nanotechnol.* **2009**, *4*, 674. (i) Li, L.; Gao, P.; Schuermann, K. C.; Ostendorp, S.; Wang, W.; Du, C.; Lei, Y.; Fuchs, H.; Cola, L. D.; Müllen, K; Chi, L. *J. Am. Chem. Soc.* **2010**, *132*, 8807. (j) Fabiano, S.; Musumeci, C.; Chen, Z.; Scandurra, A.; Wang, H.; Loo, Y.; Facchetti, A.; Pignataro, B. *Adv. Mater.* **2012**, *24*, 951. (k) Tanase, C.; Meijer, E. J.; Blom, P. W. M.; de Leeuw, D. M. *Org. Electron.* **2003**, *4*, 33.

(3) (a) Xu, G.; Bao, Z.; Groves, J. T. *Langmuir* **2000**, *16*, 1834. (b) Sanderg, H. G. O.; Frey, G. L.; Shkunov, M. N.; Sirringhaus, H.; Friend, R. H.; Nielsen, M. M.; Kumpf, C. *Langmuir* **2002**, *18*, 10176. (c) Scott, J. C.; Samuel, J. D. J.; Hou, J. H.; Rettner, C. T.; Miller, R. D. *Nano Lett.* **2006**, *6*, 2916. (d) Park, B.; Aiyar, A.; Hong, J.; Reichmanis, E. *ACS Appl. Mater. Interfaces* **2011**, *3*, 1574.

(4) (a) Mativetsky, J. M.; Kastler, M.; Savage, R. C.; Gentilini, D.; Palma, M.; Pisula, W.; Müllen, K.; Samorì, P. *Adv. Funct. Mater.* **2009**, *19*, 2486. (b) Wang, S.; Dössel, L.; Mavrinskiy, A.; Gao, P.; Feng, X.; Pisula, W.; Müllen, K. *Small* **2011**, *7*, 2841.

(5) Ruiz, R.; Nickel, B.; Koch, N.; Feldman, L. C.; Haglund, R. F.; Kahn, A.; Scoles, G. *Phys. Rev. B* **2003**, *67*, No. 125406.

(6) (a) Dinelli, F.; Murgia, M.; Levy, P.; Cavallini, M.; Biscarini, F.; de Leeuw, D. M. *Phys. Rev. Lett.* **2004**, *92*, No. 116802. (b) Ruiz, A.; Papadimitratos, A.; Mayer, A. C.; Malliaras, G. G. *Adv. Mater.* **2005**, *17*, 1795.

(7) Tsao, H. N.; Cho, D.; Andreasen, J. W.; Rouhanipour, A.; Breiby, D. W.; Pisula, W.; Müllen, K. *Adv. Mater.* **2009**, *21*, 209.

(8) DeLongchamp, D. M.; Kline, R. J.; Jung, Y.; Germack, D. D.; Lin, E. K.; Moad, A. J.; Tichter, L. J.; Toney, M. F.; Heeney, M.; McCulloch, I. *ACS Nano* **2009**, *3*, 780.

(9) Lim, S. C.; Kim, S. H.; Lee, J. H.; Kim, M. K.; Kim, D. J.; Zyung, T. *Synth. Met.* **2005**, *148*, 75.

(10) (a) Kline, R. J.; DeLongchamp, D. M.; Fischer, D. A.; Lin, E. K.; Heeney, M.; McCulloch, I.; Toney, M. F. *Appl. Phys. Lett.* **2007**, *90*, No. 062117. (b) Jung, Y.; Kline, R. J.; Fischer, D. A.; Lin, E. K.; Heeney, M.; McCulloch, I.; DeLongchamp, D. M. *Adv. Funct. Mater.* **2008**, *18*, 742.